**Atmospheric
Chemistry
and Physics
Discussions**

An operational system for the assimilation of satellite information on wild-land fires for the needs of air quality modelling and forecasting

M. Sofiev[1], R. Vankevich[2], M. Lanne[1], M. Prank[1], V. Petukhov[2], T. Ermakova[2], and J. Kukkonen[1]

[1]Finnish Meteorological Institute, Erik Palmenin aukio 1, P.O.Box 503, 00101, Helsinki, Finland
[2]Russian State Hydrometeorological University, Malookhtinsky Avenue 98, 195196, St. Petersburg, Russia

Correspondence to: M. Sofiev (mikhail.sofiev@fmi.fi)

ACPD

9, 6483–6513, 2009

Fire Assimilaion System

M. Sofiev et al.

Title Page

Abstract	Introduction
Conclusions	References
Tables	Figures

|◄ | ►|
◄ | ►

Back | Close

Full Screen / Esc

Printer-friendly Version

Interactive Discussion

Fire Assimilaion System

M. Sofiev et al.

Abstract

This paper investigates a potential of two remotely sensed wild-land fire characteristics: 4-μm Brightness Temperature Anomaly (TA) and Fire Radiative Power (FRP) for the needs of operational chemical transport modelling and the short-term forecasting of the atmospheric composition and air quality. Two treatments of the TA and FRP data are presented and a methodology for evaluating the emission fluxes is described. The method does not contain a complicated analysis of vegetation state, fuel load, burning efficiency and related factors, which are comparatively uncertain but inevitably involved in approaches based on burnt-area scars or similar products. The core of the current methodology is based on the empirical emission factors that have been derived from the analysis of several fire episodes in Europe (28 April–5 May 2006, 15–25 August 2006, August 2008 etc.). These episodes were characterised by: (i) well-identified FRP and TA values, and (ii) available independent observations of aerosol concentrations and optical thickness for the regions where fire smoke was dominant in comparison with contributions of other pollution sources. The emission factors were determined separately for the forested and grassland areas; in case of mixed-type land use an intermediate scaling was assumed. Despite significant difference between the TA and FRP products, an accurate non-linear fitting between the approaches was found. The agreement was comparatively weak only for small fires where the accuracy of both products is low. The re-analysis and forecasting applications of the Fire Assimilation System (FAS) showed that both TA and FRP products are suitable for evaluation of the emission fluxes from the wild-land fires. The concentrations of aerosols predicted by the regional dispersion modelling system SILAM appear within a factor of 2–3 from observations. The main areas of improvement include further refining the emission factors over the globe, explicit determination and appropriate treatment of the type of fires, evaluation of the injection height of the plumes and predicting the fire temporal evolution.

Fire Assimilaion System

M. Sofiev et al.

1 Introduction

Each year about 5000 km^2 of forested land in Europe is burned by more than 50 000 fires. The wild-land fires occur in all European countries, being particularly intensive in the arid southern and eastern regions. Globally, vast forests of Russia and Brasilia, as well as central Africa are among the most severely affected areas. Total estimates of the consumed biomass vary widely, usually rangin between 5 and 10 Gtons annually (Scholes and Andreae, 2000; Chin et al., 2002).

Regional specific of the fires adds-on to the complexity of the phenomenon. For instance, in forested regions the main impact and the amount of consumed biomass can be attributed to a comparatively small number of major episodes, while e.g. in Africa and in arid regions a typical intensity of individual fires is usually smaller but their count is much larger (Schultz et al., 2008). The impact of fires on climate processes, atmospheric composition and air quality also varies widely from region to region and its estimates may differ significantly between different studies (e.g. Barbosa et al., 1999; Wotawa et al., 2001; Schultz, 2002; Generoso et al., 2003; Duncan et al., 2003; Soja et al., 2004; van der Werf et al., 2004; Schultz et al., 2008).

At present, most of the fires are ignited by humans, either deliberately or accidentally. It is, therefore, difficult to make any quantitative predictions regarding individual fire events. The forecasting capability of various fire indices is therefore limited, although they can be successfully correlated with the probability of the ignited flames to develop into a full-scale fire (Tanskanen and Venäläinen, 2008). Presently, a widely used methodology for obtaining the fire information for real-time applications is based on the operational in-situ and remote sensing observations of active fires – using fire monitoring towers, aircrafts or satellites.

There are two main types of remote-sensing information that are suitable for assessing the features and impacts of fires. Most of the above-mentioned studies are based on the analyses of burnt areas, which are performed on a monthly or, rarely, half-monthly basis. The other type of input data is based on surface temperature ob-

servations and their derivatives.

One of the early operational Fire Alarm Systems based on satellite information has been developed in Finland in mid-1990s and is still operational (http://virpo.fmi.fi/ metsapalo_public/firemap/fires.html). The system utilizes the hot-spot information from the AVHRR and AATSR instruments and generates alarm messages for the author-ities and fire-fighting services if an overheated pixel (compared to the neighbouring ones) appears anywhere in Finland. However, the system provides only qualitative in-formation (the appearance of a fire) and does not describe its intensity or the chemical composition of the emission.

The goal of the current paper is to present a new-generation Fire Assimilation Sys-tem (FAS), which evaluates globally the emission fluxes originated from wild-land fires with a daily resolution. The predicted emissions in Europe are subsequently utilized by the chemical transport model SILAM (http://silam.fmi.fi, Sofiev et al., 2006) for forecast-ing and past-time assessment of the atmospheric composition. This SILAM application also enables the indirect verification of the FAS itself via comparison of modelled con-centrations with in-situ and remote-sensing observations.

2 Background

The FAS is based on Level 2 MODIS Collection 4 and 5 Active Fire Products, which are used for the near-real-time and historical evaluation of the emission from wild-land fires. This information is processed into the emission input for the atmospheric composition modelling system SILAM for a subsequent evaluation of the impact of fires on atmospheric composition and air quality.

Present FAS consists of two parallel branches based on semi-independent products: the Temperature Anomaly and Fire Radiative Power. Their main idea and processing towards the emission fluxes of atmospheric pollutants are described further, starting from the outlines of the corresponding fire products.

◄ | ►

◄ | ►

Back | Close

Full Screen / Esc

Printer-friendly Version

Interactive Discussion

2.1 The fire detection algorithm of the MODIS instrument

The MODIS fire detection procedure is based on a contextual algorithm of Giglio et al. (2003) that exploits the strong emission of mid-infrared radiation from fires (Dozier, 1981; Matson and Dozier, 1981). The algorithm examines each pixel of the MODIS
5 swath, and attributes it to one of the following classes: missing data, cloud, water, non-fire, fire, or unknown. For each fire-classified pixel, the procedure attempts to use the neighbouring pixels to estimate the radiometric signal of the pixel if there would be no fire there. Valid neighbouring pixels are identified in a window centred on the potential fire pixel and subsequently used to estimate this background value. If the
10 background characterization is successful, a series of contextual threshold tests are used to confirm the active-fire hypothesis. These look for the characteristic signature of an active fire in which both the $4\,\mu$m brightness temperature and the difference between the 4 and $11\,\mu$m brightness temperatures depart substantially from that of the non-fire background. The thresholds are adjusted based on the natural variability
15 of the background. Additional specialized tests are used to eliminate false detections caused by sun glint, desert boundaries, and errors in the water mask. Candidate fire pixels that are not rejected in the course of these tests are assigned with the class of fire.

2.1.1 The Temperature Anomaly (TA)

20 For a simple fire-detection purposes, the fire-classified pixel is attributed with its 4-μm brightness temperature. The method is also known as hot-spot counting and the pixel temperature is further referred in this study as the TA-value.

    The simplicity of this product and its operational availability allowed its utilization as a starting point for FAS development. This branch is hereinafter referred to as FAS-TA.
25 The system receives the input from ASCII telegrams that contain the location, the temperature and the detection confidence of the thermal anomalies (the T_4 brightness temperature). This brightness temperature is then multiplied with an empirical coefficient

of 6.78 ton yr^{-1} K^{-1} to yield an emission flux of PM$_{2.5}$ (Saarikoski et al., 2007). The advantages of the scheme are its simplicity and the Near-Real-Time (NRT) availability of the data, which allow its fast implementation. However, the information obtained from the TA value is quite limited since the algorithm neglects the background temperature
5   of the fire pixels.

2.1.2   The Fire Radiative Power (FRP)

For more sophisticated reporting, the MODIS product list includes the Fire Radiative Power (FRP, a rate of release of Radiation Energy, FRE) of the fire pixel based on the empirical formula after Kaufman et al. (1998):

10    $$\text{FRP} = 4.34 \times 10^{-13} (T_4^8 - T_{4b}^8), \text{ [Watt]} \tag{1}$$

where the T_4, and T_{4b} are the fire and the background (taken from neighbouring pixels) temperatures, respectively, measured at the wave-length channel of 3.96 μm. The dependence has been obtained from fitting the actual release of radiative energy from a fire and its apparent temperature at 4 and 11 μm channels – as observed by the
15   MODIS instrument. The relationship showed good correlation for open moderate-to-strong fires. Potential difficulties may show up for small fires, partly overshadowed by trees, smouldering, etc.

     As TA, the FRP data are included into the level 2 Fire Products (MOD14 for Terra and MYD14 for Aqua satellites) and are available with comparatively short delay (usually
20   within 1–2 days), which makes it possible to utilise them within the FAS. However, FRP is not available via the Rapid Response System that is practically NRT and updated several times a day. According to experience, this can cause certain extra delays in case of some technical problems at the central processing or distribution sites.

     To convert the FRP to emission fluxes we used a similar approach as for TA – a
25   direct conversion of FRP using an empirical scaling to emission rates. In the current FAS it follows Ichoku and Kufman (2005) who related the FRP in [W] per pixel to total particulate matter (PM) emission in [kg s^{-1}].

The key parameter for FAS-FRP is therefore the emission rate of total PM per unit FRP, i.e. the smoke emission coefficient C_e [kg J^{-1}]. According to Ichoku and Kaufman (2005), C_e varies from 0.02–0.06 kg/MJ for boreal regions, 0.04–0.08 kg/MJ for Africa (mainly savannas and grassland), and 0.08–0.1 kg/MJ for Western Russian regions.

5   Since the C_e determination involved a very crude estimate of atmospheric transport (based on wind at a constant height and not involving real dispersion model), the authors suggested that the coefficients are probably overestimated by about a factor of 2. Using these estimates as the starting point, we have developed the emission coefficients that are based on actual land-cover information rather than on geographical

10   region.

2.2   Connecting the FRP emission factors and the land use

The procedure of linking the FRP products with the land-use was made in three steps.
Firstly, the LANDSAT land use inventory for Europe (used as a test domain) with 250 m resolution was aggregated to the map of the vegetation fractionation with 10 km

15   resolution. It included only three types of land use: grass and agriculture land, forests, and a mixture of these (Fig. 1).
Secondly, for these three types, we assumed three gradations of the total-PM emission coefficients: 0.1 kg MJ^{-1} for forest, 0.05 kg MJ^{-1} for grass/agriculture lands, and an average of 0.08 kg MJ^{-1} for mixed areas. These values were deduced from the

20   prevailing land cover in the domains processed by Ichoku and Kaufman (2005).
Thirdly, a limited number of well-determined fire episodes in April–May and August of 2006 in Europe was selected, for which the actual location of most of the fire pixels was attributed to one of the land cover types for each day (see spatially integrated emission flux for 2006 fire season in Europe in Fig. 2). The criteria for the selection

25   was a homogenous land use in the fire areas, sufficient episode duration (up to a week for some cases) to average out the random fluctuations in the model simulations, and the dominant contribution of fire plumes compared to other sources.
For these episodes, the generated emission was submitted to the chemical trans-

port model SILAM, which simulated the atmospheric dispersion of the plumes. The results were compared with the PM$_{2.5}$ in-situ concentrations at Finnish stations Helsinki-Kumpula (urban background), Uto (regional background), Virolahti (regional background), Oulu (small city, urban background), Vaasa (small city, urban background) and the satellite observations (MODIS AOD). The systematic deviations of both column-integrated and near-surface PM concentrations were attributed to the emission scaling.

The main reference dataset used for the calibration was the aerosol optical depth from MODIS converted to the total column-integrated PM concentrations (an extension of the MODIS AOD product available e.g. via Giovanni framework http://daac.gsfc.nasa.gov/techlab/giovanni). This dataset was utilised for setting-up the emission factors. The in-situ observations from the Finnish observational network were involved as an independent data for checking the obtained parameterizations. Such type of comparison was made by Saarikoski et al. (2007). The main reason for using the satellite observations as the main source of information for the system calibration is that the modelled near-surface concentrations are sensitive to boundary layer description in SILAM. In addition, the ground-based observational network is comparatively scarce and there are limitations due to the limited site representativeness.

We assumed that inside the fire plumes the AOD was entirely dominated by the biomass-burning products. It is supported by e.g. Saarikoski et al. (2007), who found that more than 80% of PM$_{2.5}$ during a specific episode in May 2006 was originated from fires. We therefore attributed all systematic discrepancy between the observed and calculated column AOD to errors in the emission rates – and corrected the emission factors accordingly.

The resulting emission coefficients for European domain are the following: 0.05 kg MJ^{-1} for forest, 0.025 kg MJ^{-1} for grassland and agriculture, and 0.0375 kg MJ^{-1} for mixed areas.

The resulting total emission values for Europe show that on the average in 2006–2008 the mean European daily PM$_{2.5}$ emission was ∼7.5 kton day^{-1}. This number can be compared with ∼9 kton day^{-1} of anthropogenic PM$_{2.5}$ emission reported by Euro-

pean Monitoring and Evaluation Programme EMEP (Vestreng et al., 2006). According to these values, the total European fire-related PM emission during these 3 years is nearly the same as that of the primary PM. Both anthropogenic and fire emission estimates are uncertain (Vestreng et al., 2006) and the fire emission varies from year to year (e.g. Van der Werf et al., 2006) but one can still conclude that in Europe the fire contribution to PM were comparable with the anthropogenic part during recent years.

2.3 Cross-calibration of the TA-based FAS against FAS-FRP

As seen from the above-described physical basis, the FRP approach has a clear advantage over TA. Indeed, the release of radiative energy is directly proportional to the number of carbon atoms oxidised per second. The same is true for the emission total flux. Compare to that, the dependence of the brightness temperature on the fire intensity is much less straightforward. It is also stronger affected by the external factors (e.g., meteorology), which reduce the sensitivity of the TA value to the fire intensity and actual emission.

Figure 3 illustrates these differences using the 2006 fire season as an example. As one can see, the TA mechanism is much less sensitive to the intensity of a single fire reporting most of them to be about the same intensity (the marker size is proportional to TA value), while FRP reflects the diversity.

However, FRP has its own limitations. Firstly, it is presently available from few instruments. TA, to the opposite, is a simple ground brightness temperature, which is available from a wide range of instruments and satellites. Secondly, the 11-μm channel needed for computations and for distinguishing between the types of burning is quite noisy. Thirdly, the reliance on neighbouring pixels for the background temperature of the burning one can lead to problems, especially in the regions with heterogeneous land use or densely located fires occupying more than one grid cell. Fourthly, the 8-th power of temperatures (1) makes the final estimates sensitive to inherent noise in the temperatures, thus making the FRP assessment uncertain. Finally, due to a more sophisticated algorithm the near-real-time availability of FRP from MODIS appeared

worse than that of TA reported through the Rapid Response System. In-summary, the FRP tends to loose or reports with large uncertainty the poorly seen small-scale fire events, overshadowed fires in forests, etc.

Therefore, it is reasonable to consider the inter-connection of the FAS-TA and FAS-FRP algorithms. For these purposes we used the same dataset of 2006 and took into account the split between the three land-use types.

As seen from the TA-FRP scatter plot in Fig. 4, there is a well-defined functional dependence between the TA and FRP products, with very narrow spread for moderate and strong fires. The noticeable scatter existing for small fires is to be expected because TA does not include the background temperature, which becomes comparable with actual temperature of the pixel if the fire-induced heat release is small. It is also seen from the Fig. 4 that separation of the land use types significantly improves the agreement even for small fires, especially over the forested areas.

Strong connection between FRP and TA with minor scatter allows a direct polynomial fitting of TA to FRP (Fig. 5):

$$FRP = 8.3338 \times 10^{-5} \times TA^3 - 6.11707 \times 10^{-2} \times TA^2 + 14.8674 \times TA - 1150.92 \qquad (2)$$

where TA is in [K] and FRP is in [MW].

With this fit, the scatter plot of FRP and FRP-from-TA is practically linear, with the regression slope deviating from unity by $\sim$2% and the correlation coefficient of $\sim$0.94 (Fig. 6). This non-linear transformation of TA allows its utilization as a substitution for FRP if the latter one is unavailable.

2.4 Operational setup of FAS at FMI

With the above-discussed limitations and advantages of each of the approaches, the setup for operational FAS was chosen to utilize the advantages of both TA- and FRP-based algorithms.

For the periods when both TA and FRP are available, the branches are kept independent. Each line uses its own linear scaling to emission of $PM_{2.5}$, which is then scaled

to a full list of chemicals following Andreae and Merlet (2001). For days where the FRP data are either unreliable or do not exist, the system recalibrates TA to FRP using the fitting (2). Then this FRP substitution is treated the same way as the original FRP: scaled to $PM_{2.5}$ emission and then to fluxes of other species.

⁵ Atmospheric composition forecasts require also forecasts of the fire developments, which are presently based on persistency assumption: the fires observed during the last available day in the satellite dataset are assumed to continue for the whole forecasting period with constant mean intensity.

A significant challenge for the current FAS algorithm is the diurnal variation of the fire

¹⁰ intensity. The main source of information – the MODIS instrument onboard of Aqua and Terra satellites – can provide only 2–4 values per day and only during daytime. This is evidently insufficient for the quantitative representation of the diurnal variation. Therefore, we assumed a conservative diurnal variation, same for all types of vegetation, which suggests day-time emission intensity to be 25% higher than the daily-mean level

¹⁵ while night-time emission is 25% lower (Saarikoski et al., 2007). The actual variation is most-probably larger but the construction of region-specific quantitative parameterization would require information from geostationary satellites and dedicated modelling studies. Such type of information is becoming available but so the present system uses this conservative and simple approximation.

²⁰ The fire-induced emission obtained from each branch is merged with other pollution sources taken into account by the SILAM dispersion simulations – as maps of gridded daily-mean emission rates with superimposed fixed diurnal cycle.

The SILAM modelling system (Sofiev et al., 2006) currently includes both Lagrangian and Eulerian dynamic kernels. It takes into account up to 8 different types of the trans-

²⁵ ported species including size-segregated aerosol, sulphur and nitrogen oxides and some VOCs. Operationally, it is used to predict sulphur and nitrogen oxides, ammonium, some hydrocarbons, ozone, sea salt, fine and coarse primary anthropogenic aerosols $PM_{2.5}$ and PM_{10}, as well as biogenic primary aerosols, such as pollen. The other compounds are utilised only in research applications.

Injection height for all the fires is prescribed. According to available literature data (Trentmann et al., 2006; Freitas et al., 2007; Zilitinkevich et al., 2006; Labonne et al., 2007; Mazzoni et al., 2007; Kahn et al., 2008, etc.), simulations with the BUOYANT plume-rise model (Nikmo et al., 1999), the US fire injection height archive derived from MISR observations (Mazzoni et al., 2007), the plumes from small or moderate fires very rarely rise higher than twice the height of the boundary layer H_{ABL}, being in most cases confined within 0.5–1 of H_{ABL}, especially if it is deep. Therefore, for the European fires we assumed that 50% of the emission is injected in the lowest 90 m while the rest is homogenously distributed from 90 m up to 1.1 km.

2.5 Examples of the simulations and comparison with the MODIS and ground-based observations

Two examples of the simulations with calibrated emission rates are shown in Figs. 7 and 8 where the left-hand panel presents the SILAM computations with FAS-TA emission fields for $PM_{2.5}$, the middle panel – for FAS-FRP and the right-hand panel is obtained from merged MODIS Aqua and Terra aerosol column-integrated mass over land. In the model simulations, only the fire emission is taken into account.

Analyzing these results, one has to allow for the following inherent limitations in modelling and experimental data. Firstly, the model emission fields included only aerosol released from fires while observations do not distinguish between the different sources, thus include also the anthropogenic aerosol, dust, etc. Therefore, only the area dominated by the fire plume should be compared. In addition, the actual MODIS observations of Aqua and Terra take place about two hours one after another in the morning of each day. Since each overpass covers only a part of the computation domain, the complete map is actually a compilation of several overpasses, about 1.5 h after each other. This results in certain imbalance of the merged AOD fields – both between each other and with the model. In the Figs. 7 and 8 we conditionally attributed all observations to 00:00 and 10:00 of the model time, respectively. Finally, observations do not provide any information for the areas covered by clouds or by dense aerosol plumes

(often for fires) misinterpreted as clouds.

The absolute level of predicted column-integrated PM mass differs by less than 20% from observations (e.g. in Fig. 7 slightly over $35\,\mathrm{cg\,m^{-2}}$ in the predicted peak compared with $\sim 30\,\mathrm{cg\,m^{-2}}$ observed). The shapes of the fire plume are qualitatively similar, ex-
5   cept for the northern part of the fire plume where it mixes-up with the anthropogenic pollution from Central and Eastern Europe and is getting partly overshadowed by clouds.

Figure 8 illustrates the FAS+SILAM operational forecasts for 2008 of fire-induced column-integrated concentrations, in comparison with the corresponding MODIS variable. Comparing the absolute levels with Fig. 7, one can see that fire plumes in Eastern
10   Europe in August 2008 predicted by SILAM result in about the same aerosol column burden as the anthropogenic sources. However, in the South-Eastern Europe these plumes were dominant, especially in the northern part of Ukraine, Southern Russia, but also over the Balkan area. That day, MODIS observed somewhat lower values than those predicted by SILAM. The model over-estimation was about 20%, with over
15   $50\,\mathrm{cg\,m^{-2}}$ predicted from fires against under $40\,\mathrm{cg\,m^{-2}}$ observed from all sources (but in fire-dominated area).

To build a scatter-plot of the FAS+SILAM agreement with MODIS for each day in the spring fire episode of 2006, an area with dominating fire-induced pollution has been selected out of the whole domain. Scatter plots were then made for each day
20   (see example in Fig. 9) generally showing a moderate scatter. However, day-by-day variation is large, as seen from the episodes depicted in Fig. 7 and 8. For instance, 5 March 2006 (Fig. 7) the predicted values were lower than the observed ones, while during the previous day both TA and FRP approaches showed too high emission. In general, the over-estimation was observed more often than under-estimation.
25   Comparing the scatter plots in Fig. 9 one can also notice the difference between the results of FAS-TA and FAS-FRP. The temperature-anomaly based scatter plot tends to be more homogenous and somewhat wider spread while FRP-based comparison shows stronger collapse of the points towards certain dependencies – but also larger number of outliners and stronger non-linearity visible in the plot.

An evaluation of a full pollution pattern for the episode requires consideration of anthropogenic and natural pollutants. When included, they allowed computation of quality scores for each day using MODIS AOT as an observational dataset and SILAM total AOT as a modelled one. The quantitative scores, such as a spatial correlation coefficient, figure of merit in space, RMSE and bias, are shown in Fig. 10 for the whole episode of April–May 2006. There are several peculiarities of this comparison. Each day, a substantial fraction of the MODIS maps is left undefined due to clouds where the concentrations are usually somewhat lower due to scavenging. This caused an unknown and changing day-to-day bias towards the higher area-mean AOT of the MODIS maps. The presented SILAM run was missing the boundary conditions for the sea salt, which resulted in strong under-estimation of AOT over Atlantic Ocean. Altogether, these peculiarities have offset the eventual positive bias over the fire-dominated areas and resulted in small under-prediction of the mean AOT value (Fig. 10).

3 Discussion

The Fire Assimilation System presented above is based on a simple set of assumptions and involves explicit TA/FRP-to-emission scaling factors. A similar approach was used by e.g. Ichoku and Kaufman (2005) for determining the initial set of emission factors. However, in that work the assumptions regarding the transport of smoke from the fires were extremely simple. According to the authors, such simplification results in uncertainties in the emission coefficients of about a factor of 2, with a probable over-prediction of the emission factor C_e.

In this study, the detailed transport simulations are expected to result in a higher accuracy of the scaling. For the European area, we found that the C_e values of Ichoku and Kaufman are indeed over-estimated, but somewhat more than was expected: on the average, our factors are 2–3 times lower. However, the new coefficients are still based on a fairly limited set of data and longer-term analysis is needed to refine these.

Other sources for comparison are the existing fire inventories performed using in-

dependent approaches, such as Global Fire Emission Database v.2 (GFEDv2, Giglio et al., 2006) or RETRO archive (Schultz et al., 2008). Average fire-related emission of $PM_{2.5}$ in Europe for 1997–2005, according to GFEDv2, was ~1 kton day^{-1}, i.e. a factor of 7.5 lower than the values obtained in this study. However, according to Giglio et al. (2006), the GFEDv2 data should be considered as conservative estimates. The RETRO analysis stops in 2000 when they showed fluxes, which are more than twice as high as those of GFEDv2 – 2.1 kton day^{-1} – but still more than 3 times lower than the result of this study. However, the comparison with both GFEDv2 and RETRO is uncertain because both inventories cover the period before 2006. A series of record-strong fire events in spring 2006 (Russian fires), in summer 2007 (Southern European and Greek fires) and 2008 (south-eastern fires) could largely be responsible for the differences.

As a summary for the emission factor evaluation, the current methodology shows the results between the estimates of GFEDv2 and RETRO and the original Ichoku and Kaufman emission factors. The comparison of the atmospheric dispersion predictions and with in-situ and remote-sensing observations showed that the scores varied day by day, depending on the particular episode and region. Studies over longer periods and wider areas are needed to refine the emission factors.

An evaluation of the vertical distribution of the initial plumes comprised another difficult challenge for the system. Most small and moderate fires do not create plume buoyancy sufficient to reach substantially further than the top of the boundary layer. However, for the large-scale fires this may not be the case. Freitas et al. (2007) showed that injection height can exceed 5–7 km, especially if atmospheric conditions are favourable and the fires are very strong. The authors also stressed the significant impact of the latent heat flux, which can almost double the plume elevation in some cases. However, very strong fires are rare in the European conditions and have not occurred during the considered period of 2006–2008.

For most of moderate- and small-scale fires, simple parameterizations based on the boundary layer height (or even a prescribed fixed distribution) may provide reasonable

estimates without major inaccuracies. In the sensitivity simulations performed within this study, a change of the maximum injection height from 100 m to 1500 m resulted in about ~2.5-fold decrease of the upper percentile (98%) of concentrations (computed with regard to different meteorological situations) at a distance of 60 km from the point source placed in Central Europe. The sensitivity decreases with growing distance from the source and becomes less than 10% at a distance of ~250 km. For lower percentiles, the change is substantially smaller also in the vicinity of the source. A reasonable assumption for small and moderate fires is therefore that at least 50–75% of emission flux is distributed within the boundary layer while the rest is injected slightly above it.

Analysis of performance of FAS-TA and FAS-FRP did not reveal an unequivocally better approach. As seen from examples of Figs. 3, 7, 8, the difference between the emission estimates for the same region and time, can be as large as a factor of several times. These differences are to be related to the retrieval algorithms. Contrary to TA, FRP depends on background temperature determined from eight surrounding pixels (providing that they are not overheated themselves) and the actual pixel temperature, both taken to the 8-th power. A single hot pixel surrounded by the colder ones is therefore reported as an intensive fire with a high emission rate. On the other hand, emission from widespread small-scale fires may be under-estimated due to a smaller temperature differences between the adjacent pixels. Smaller difference would also lead to lower signal-to-noise ratio and to more uncertain emission estimates.

The TA-based assessments are probably vulnerable to a mirroring problem: the algorithm ignores background temperature, which are used only for classification of the fire pixels. Consequently, the TA-method does not report the emission below certain level corresponding to commonly occurring temperatures in the region. But neither is it sensitive to large fires – because the brightness temperature grows slower than linearly with the fire intensity (expressed as number of carbon atoms oxidised per second).

In a general case, the FRP algorithm tends to report high emission from few strong spots among the comparatively low-emitting small fires. The TA approach, to the opposite, better detects small fires potentially under-estimating the emission from the strong

Printer-friendly Version

Interactive Discussion

ones. However, in real applications these differences are partly averaged over thousands of fire pixels analysed for each day. As a result, the regional emission estimates from TA and FRP are usually comparable. Experience of the SILAM-based verification did not give strong favour to either of the methods. For instance, the comparison in Fig. 9 reflects the day when the TA-based computations were somewhat preferable. However, during the next day (not shown) the FRP-based computations were in better agreement with the observations.

A potential way to improve the emission estimates for individual fires is to use the 11-μm channel to distinguish between the open flames and smouldering. However, this channel is noisier than the 4-μm one and the characteristic correlations with the type of the fire are not very high. This approach is therefore not implemented in the current FAS version.

4 Conclusions

The presented Fire Assimilation System consists of two branches based on partly complementary treatments of the remote-sensing information on the wild-land fires: the Temperature Anomaly and Fire Radiative Power. The output variables of these methods are not entirely independent and can be reasonably well fitted one to another for moderate and strong fires, for which the background temperatures of non-burning pixels are much smaller than the temperatures of the burning ones.

The procedure of determination of the emission factors for the FAS-FRP branch is based on the approach of Ichoku and Kaufman (2005). However, in the current work the dispersion of the fire plumes was computed by the chemical transport model SILAM. The model predictions combined with the satellite observations of column-integrated optical density and aerosol mass allowed a significant refinement of the emission factors suggested by Ichoku and Kaufman (2005). The new factors were shown to be lower by 2 to 3 times, which is in correspondence with analysis of Ichoku and Kaufman, who suggested that their estimates can be too high.

The main inherent uncertainties of the FAS presented in this study include: (i) a simplified land use segregation, (ii) consideration of just one type of fires, (iii) conservative diurnal variation of the fire intensity, and (iv) a simplified treatment of the vertical profile of the emission fluxes. The systematic deviations in vertical profile of the SILAM concentrations could result in 10–20% of under-estimation of the transport speed and the emission factors.

The described FAS has been implemented in the operational air quality forecasting suite of the Finnish Meteorological Institute and used since 2006. The simulations are routinely compared with available in-situ and remote-sensing observations and generally are in agreement with the observations over the areas, for which the fire-induced pollution is dominant. The difference of the peaks of column-integrated concentrations from the observations characteristically range from 20% to 50%. However, in specific cases of misinterpretation of land-use or fire type, the difference can be substantially higher.

References

Andreae, M. O. and Merlet, P.: Emission of trace gases and aerosols from biomass burning, Global Biogeochem. Cy., 15, 955–966, 2001.

Barbosa, P. M, Stroppiana, D., Gregoire, J. M., and Pereira, J. M. C.: An assessment of vegetation fire in Africa (1981–1991): Burned areas, burned biomass, and atmospheric emissions, Global Biogeochem. Cy., 13(4), 933–950, 1999.

Chin, M., Ginoux, P., Kinne, S., Torres, O., Holben, B. N., Duncan, B. N., Martin, R. V., Logan, J. A., Higurashi, A., and Nakajama, T.: Tropospheric aerosol optical thickness from the GO-CART model and comparison with satellite and sun photometer measurements, J. Atmos. Sci., 59, 461–483, 2002.

Full Screen / Esc

Printer-friendly Version

Interactive Discussion

Dozier, J.: A method for satellite identification of surface temperature fields of subpixel resolution, Remote Sens. Environ., 11, 221–229, 1981.

Duncan, B. N., Martin, R. V., Staudt, A. C., Yevich, R., and Logan, J. A.: Interannual and seasonal variability of biomass burning emissions constrained by satellite observations, J. Geophys. Res., 108(D2), 4100, doi:10.1029/2002JD002378, 2003.

Generoso, S., Bréon, F.-M., Balkanski, Y., Boucher, O., and Schulz, M.: Improving the seasonal cycle and interannual variations of biomass burning aerosol sources, Atmos. Chem. Phys., 3, 1211–1222, 2003, http://www.atmos-chem-phys.net/3/1211/2003/.

Giglio, L., Kendall, J. D., and Mack, R.: A multi-year active fire dataset for the tropics derived from the TRMMVIRS, Int. J. Remote Sens., 24(22), 4505–4525, 2003.

Giglio, L., van der Werf, G. R., Randerson, J. T., Collatz, G. J., and Kasibhatla, P.: Global estimation of burned area using MODIS active fire observations, Atmos. Chem. Phys., 6, 957–974, 2006, http://www.atmos-chem-phys.net/6/957/2006/.

Freitas, S. R., Longo, K. M., Chatfield, R., Latham, D., Silva Dias, M. A. F., Andreae, M. O., Prins, E., Santos, J. C., Gielow, R., and Carvalho Jr., J. A.: Including the sub-grid scale plume rise of vegetation fires in low resolution atmospheric transport models, Atmos. Chem. Phys., 7, 3385–3398, 2007, http://www.atmos-chem-phys.net/7/3385/2007/.

Ichoku, C. and Kaufman, J. Y: A Method to Derive Smoke Emission Rates From MODIS Fire Radiative Energy Measurements, IEEE T. Geosci. Remote, 43(11), 2636–2649, 2005.

Kahn, R. A, Chen, Y., Nelson, D. L., Leung, F-Y., Li, Q., Diner, D. J., Logan, J. A.: Wildfire Smoke Injection Heights – Two Perspectives from Space, Geophys. Res. Lett., 35, L04809, doi:10.1029/2007GL032165, 2008.

Kaufman, Y. J., Justice, C. O., Flynn, L. P., Kendall, J. D., Prins, E. M., Giglio, L., Ward, D. E., Menzel, W. P., and Setzer, A. W.: Potential global fire monitoring from EOS-MODIS, J. Geophys. Res., 103, 32215–32238, 1998.

Labonne, M., Bre'on, F. M., and Chevallier, F.: Injection height of biomass burning aerosols as seen from a spaceborne lidar, Geophys. Res. Lett., 34, L11806, doi:10.1029/2007GL029311, 2007.

Matson, M. and Dozier, J.: Identification of subresolution high temperature sources using a thermal IR sensor, Photogramm. Eng. Rem. S., 47, 1311–1318, 1981.

Mazzoni, D., Logan, J. A., Diner, D., Kahn, R., Tong, L., and Li, Q.: A data-mining approach to associating MISR smoke plume heights with MODIS fire measurements, Remote Sens. Environ., 107, 138–148, 2007.

Nikmo, J., Tuovinen, J. P., Kukkonen, J., and Valkama, I.: A hybrid plume model for local-scale atmospheric dispersion, Atmos. Environ., 33, 4389–4399, 1999.

Saarikoski, S., Sillanpää, M., Sofiev, M., Timonen, H., Saarnio, K., Teinilä, K., Karppinen, A., Kukkonen, J., and Hillamo, R.: Chemical composition of aerosols during a major biomass burning episode over northern Europe in spring 2006: experimental and modelling assessments, Atmos. Environ., 41, 3577–3589, 2007.

Scholes, M. and Andreae, M. O.: Biogenic and pyrogenic emissions from Africa and their impact on the global atmosphere, Ambio, 29, 23–29, 2000.

Schultz, M. G., Heil, A., Hoelzemann, J. J., Spessa, A., Thonicke, K., Goldammer, J., Held, A. C., and Pereira, J. M. C.: Global Emissions from Wildland Fires from 1960 to 2000, Global Biogeochem. Cy., 22, GB2002, doi:10.1029/2007GB003031, 2008.

Scholes, M. and Andreae, M. O.: Biogenic and pyrogenic emissions from Africa and their impact on the global atmosphere, Ambio, 29, 23–29, 2000.

Schultz, M. G.: On the use of ATSR fire count data to estimate the seasonal and interannual variability of vegetation fire emissions, Atmos. Chem. Phys., 2, 387–395, 2002, http://www.atmos-chem-phys.net/2/387/2002/.

Schultz, M. G., Heil, A., Hoelzemann, J. J., Spessa, A., Thonicke, K., Goldammer, J. G., Held, A. C., Pereira, J. M. C., and van het Bolscher, M.: Global wildland fire emissions from 1960 to 2000, Global Biogeochem. Cy., 22, GB2002, doi:10.1029/2007GB003031, 2008.

Sofiev, M., Siljamo, P., Valkama, I., Ilvonen, M., and Kukkonen, J.: A dispersion modelling system SILAM and its evaluation against ETEX data, Atmos. Environ., 40, 674–685, doi:10.1016/j.atmosenv.2005.09.069, 2006.

Soja, A. J., Cofer, W. R., Shugart, H. H., Sukhinin, A. I., Stackhouse Jr., P. W., McRae, D. J., and Conard, S. G.: Estimating fire emissions and disparities in boreal Siberia (1998–2002), J. Geophys. Res., 109, D14S06, doi:10.1029/2004JD004570, 2004.

Tanskanen, H. and Venäläinen, A.: The relationship between fire activity and fire weather indices at different stages of the growing season in Finland, Boreal Environ. Res., 13, ISN 1239-6095 (print), ISN 1797-2469 (online), 2008.

Trentmann, J., Luderer, G., Winterrath, T., Fromm, M. D., Servranckx, R., Textor, C., Herzog, M., Graf, H.-F., and Andreae, M. O.: Modeling of biomass smoke injection into the lower stratosphere by a large forest fire (Part I): reference simulation, Atmos. Chem. Phys., 6, 5247–5260, 2006, http://www.atmos-chem-phys.net/6/5247/2006/.

van der Werf, G., Randerson, J. T., Collatz, G. J., Giglio, L., Kasibhatla, P. S., Arellano, A. F.,

Fire Assimilaion System

M. Sofiev et al.

Olsen, S. C., and Kasischke, E. S.: Continental-scale partitioning of fire emissions during the 1997 to 2001 El Niño/La Niña period, Science, 303, 73–76, 2004.

van der Werf, G. R., Randerson, J. T., Giglio, L., Collatz, G. J., Kasibhatla, P. S., and Arellano Jr., A. F.: Interannual variability in global biomass burning emissions from 1997 to 2004, Atmos. Chem. Phys., 6, 3423–3441, 2006, http://www.atmos-chem-phys.net/6/3423/2006/.

Vestreng, V., Rigler, E., Adams, M., Kindbom, K., Pacyna, J. M., Denier van der Gon, H., Reis, S., and Travnikov, O.: Inventory review 2006, Emission data reported to LRTAP and NEC Directive, Stage 1, 2 and 3 review and Evaluation of Inventories of HM and POPs, EMEP/MSC-W Technical Report 1/2006 ISSN 1504-6179, http://www.emep.int, 2006

Wotawa, G., Novelli, P., Trainer, M., and Granier, C.: Inter-Annual Variability of Summertime CO Concentrations in the Northern Hemisphere Explained by Boreal Forest Fires in North America and Russia, Geophys. Res. Lett., 28(24), 4575–4578, 2001.

Zilitinkevich, S. S., Hunt, J. C. R., Esau, I. N., Grachev, A. A., Lalas, D. P., Akylas, E., Tombrou, M., Fairall, C. W., Fernando, H. J. S., Baklanov, A. A., and Joffre, S. M.: The influence of large convective eddies on the surface turbulence, Quarterly Journal of the Royal Meteorological Society, 132 pp., 1423–1456, 2006.
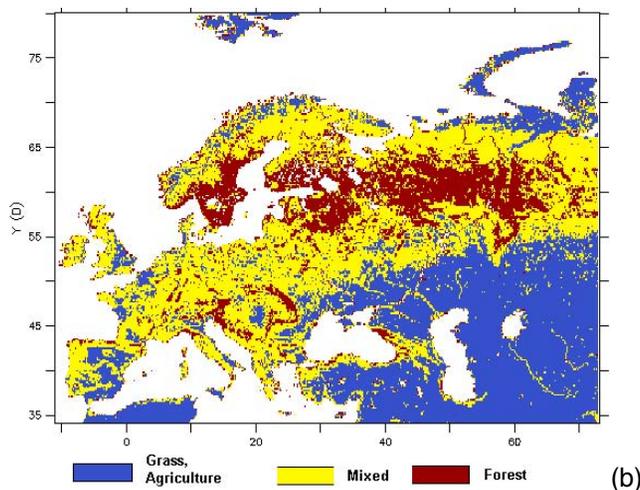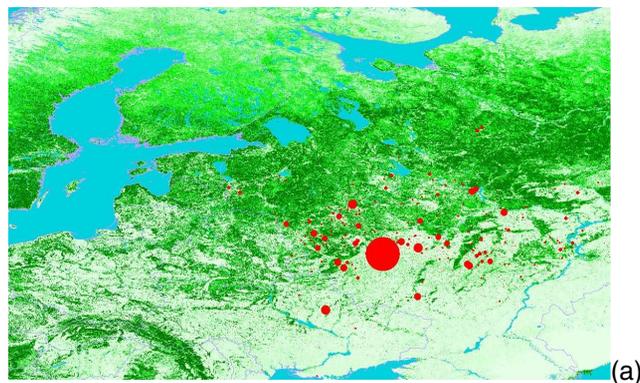
Fig. 1. Panel **(a)**: the LANDSAT land cover inventory, spatial resolution of 250 m; examples of fires in May 2006 are shown as red dots, their diameter proportional to FRP. Panel **(b)**: the classification of prevailing land types at a resolution of 10 km, as a surrogate for emission factors.
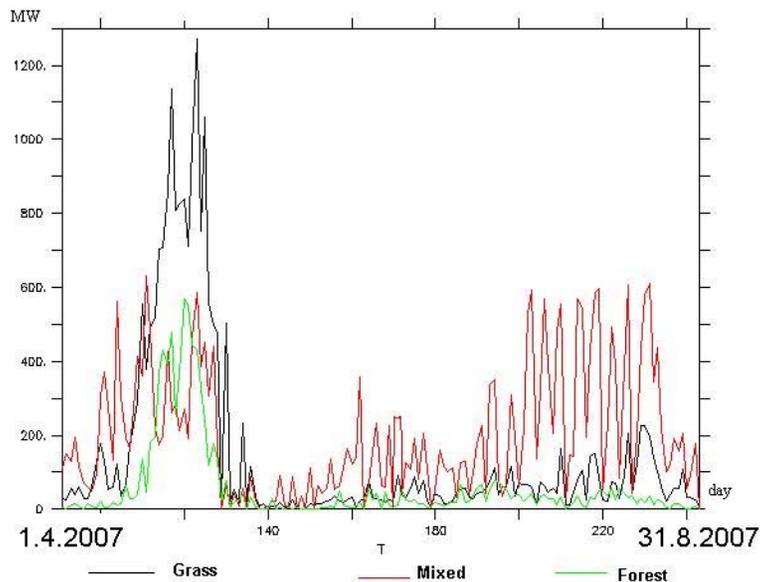
Fig. 2. Temporal evolution of fire FRP distributed between the landuse types for the fire season of 2006. Periods selected for the system calibration are end-April and mid-August.
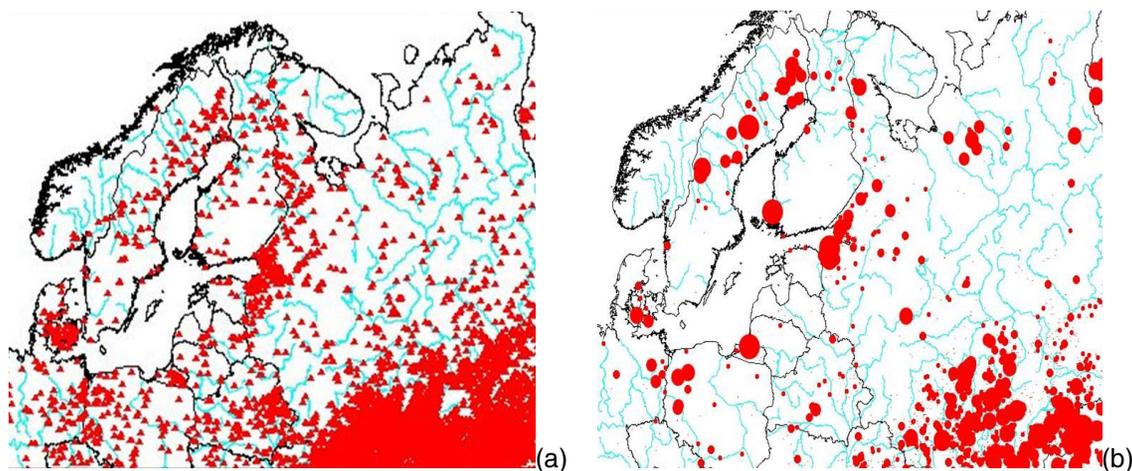
Fig. 3. TA- (left-hand panel) and FRP- (right-hand panel) based total emission estimates for May–August 2006 (relative units). The size of markers is proportional to the corresponding emission values.
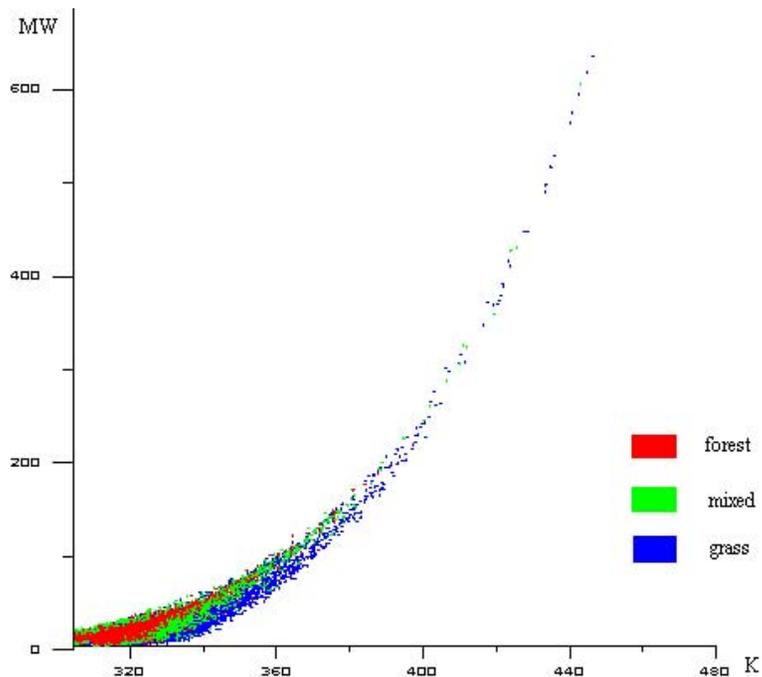
Fig. 4. The relation between the brightness temperatures, [K] from 21-st band of MODIS (horizontal axis) and FRP for the same fire pixel from MOD14 fire product [MW per pixel area] (vertical axis). Colours of the dots correspond to the land cover types (red – forest, green – mixed forest and grass, blue – grass only).
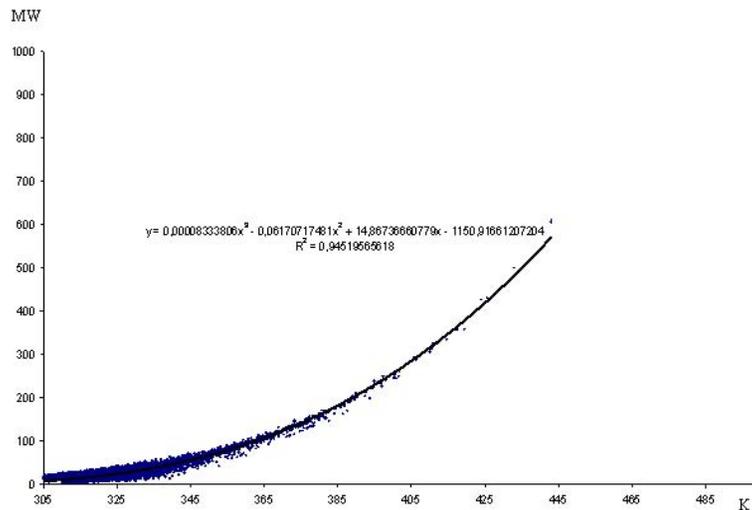
Fig. 5. Polynomial fitting of TA [K] to FRP [MW] for forest land use type. Fitting equation: $y = 8.33 \times 10^{-5} x^3 - 6.17 \times 10^{-2} x^2 + 14.9x - 1.15 \times 10^3$, $R^2 = 0.945$.
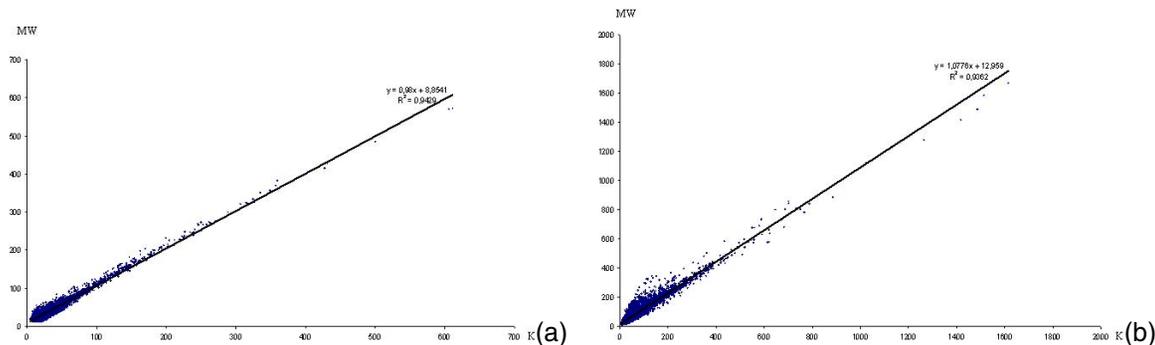
Fig. 6. Verification of TA-to-FRP polynomial fit. A scatter plot of predicted FRP from TA (using the fit shown in Fig. 5) versus the one actually observed by MODIS. Upper panel is for forest (regression: y=0.98x+8.85, R^2=0.943), lower panel is for grass (regression: y=1.078x+12.96, R^2=0.936), [MW].
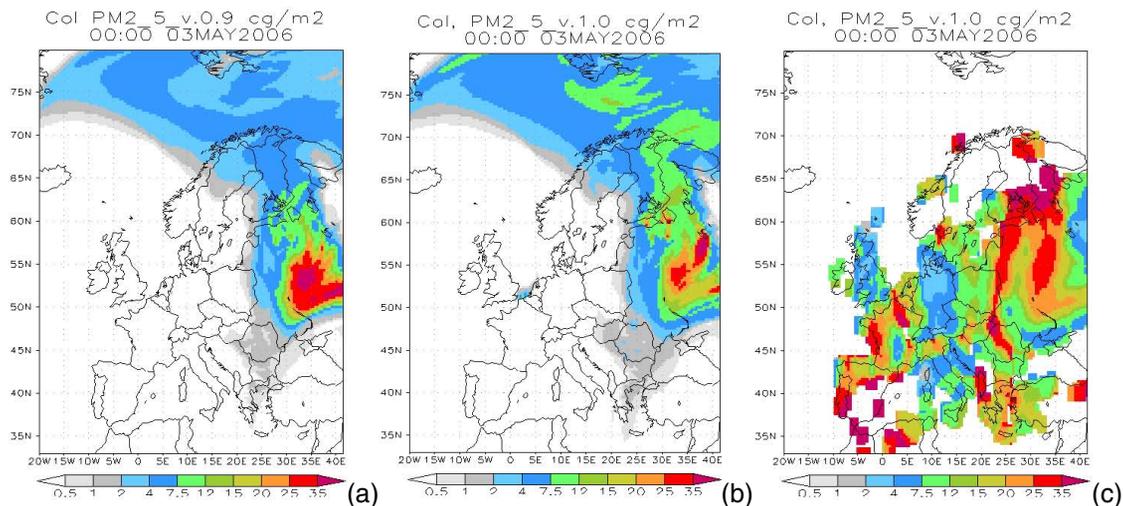
Fig. 7. Spatial distribution of column-integrated PM$_{2.5}$ concentration, 3 May 2006. Panel **(a)**: SILAM simulations with FAS-TA emission, panel **(b)**: the run with FAS-FRP emission, panel **(c)**: combined MODIS Aqua and Terra observations. Unit: (cg PM$_{2.5}$ m^{-2}).
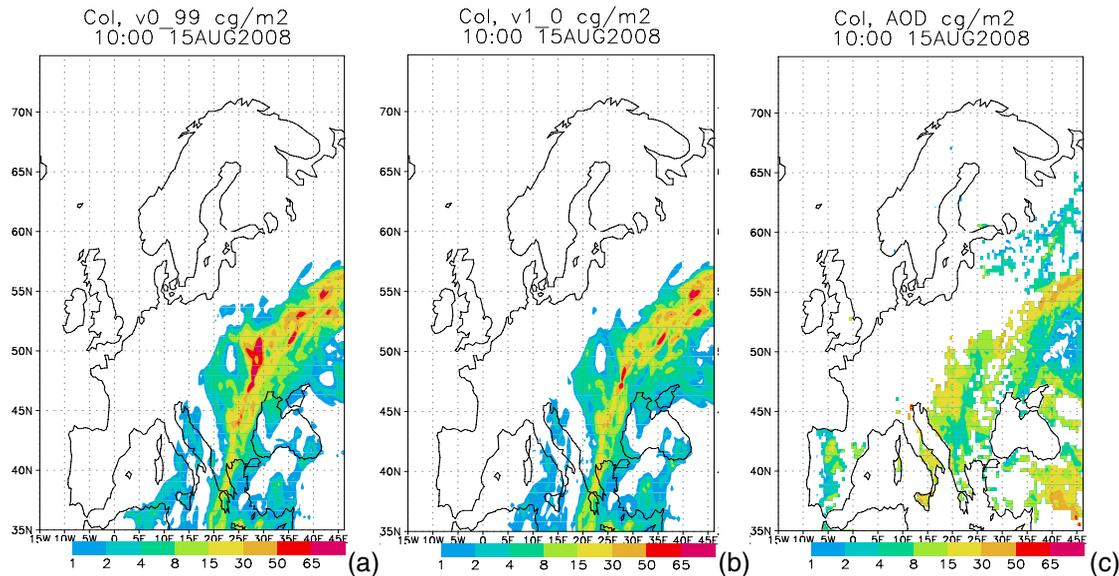
Fig. 8. Spatial distribution of near-surface concentration extracted from FAS+SILAM operational forecast. Panel **(a)** is for SILAM simulations with FAS-TA emission, panel **(b)** is for the run with FAS-FRP emission, panel **(c)** is combined MODIS Aqua and Terra observations of total PM mass in column. Note limited comparability of modelled PM from fires and observed total-PM concentrations including all sources.
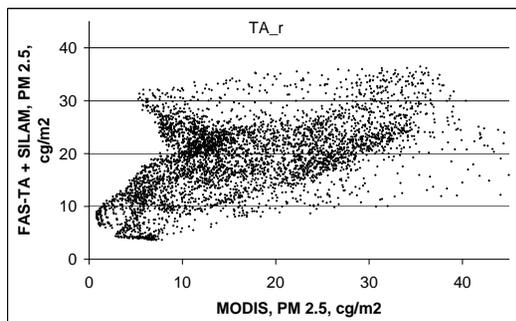
(a)
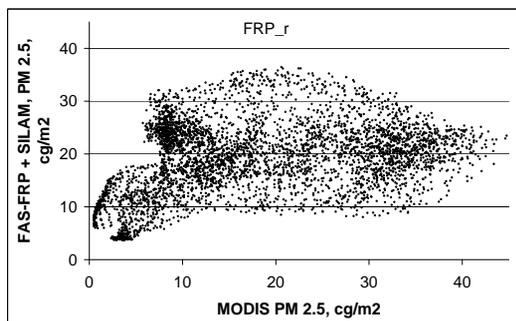
(b)

Fig. 9. Scatter-plots for TA and FRP against MODIS AOT observations (converted to $PM_{2.5}$ column load) for 3 May 2006. Only fire-dominated area is included (4557 grid cells). Mean MODIS 19 cg $PM_{2.5}$ m^{-2}, mean FAS-TA 18 cg $PM_{2.5}$ m^{-3}, mean FAS-FRP 18 cg $PM_{2.5}$ m^{-3}; correlation coefficients R_{TA}=0.5, R_{FRP}=0.3.
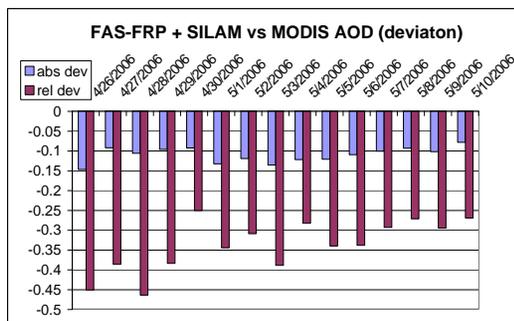
(a)
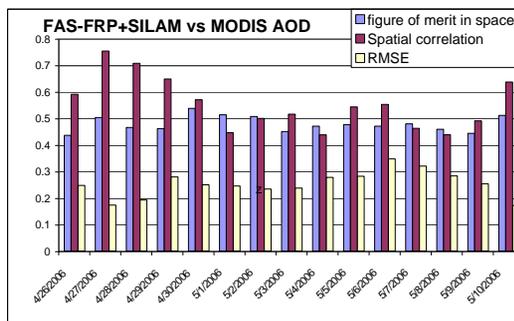
(b)

Fig. 10. Time evolution of spatial scores of SILAM AOT fields with full-chemistry simulations against MODIS AOT. Emission: FAS-FRP for fires, EMEP-2003 for anthropogenic SO_x, NO_x, NH_x, VOCs, wind-driven sea salt flux. Maps over the whole of Europe are evaluated.